R. & M. No. 3401

MINISTRY OF AVIATION

AERONAUTICAL RESEARCH COUNCIL
REPORTS AND MEMORANDA

Turbulent Flow Past Two-Dimensional Bases in Supersonic Streams

By R. C. HASTINGS

LONDON: HER MAJESTY'S STATIONERY OFFICE
1965
ELEVEN SHILLINGS NET

Turbulent Flow Past Two-Dimensional Bases in Supersonic Streams

By R. C. HASTINGS

COMMUNICATED BY THE DEPUTY CONTROLLER AIRCRAFT (RESEARCH AND DEVELOPMENT), MINISTRY OF AVIATION

*Reports and Memoranda No. 3401**
December, 1963

Summary.

Experiments on the flow past two-dimensional, rearward-facing steps with turbulent approach boundary layers have been made at Mach numbers of 1·56, 2·41 and 3·10. Wide ranges of the ratio of boundary-layer thickness to step height were covered. The flow downstream of one step was briefly explored at a Mach number of 2·41.

The base pressures are most conveniently expressed in terms of pressure-recovery coefficients for the flows downstream of the steps. Fairly good correlation of these coefficients is obtained by using the concept of local similarity upon which the measurement of skin friction by surface pitot tubes is based.

LIST OF CONTENTS

* Replaces R.A.E. Tech. Note No. Aero. 2931—A.R.C. 25 737.

LIST OF TABLES

LIST OF ILLUSTRATIONS

---

1. *Introduction.*

Despite many previous studies of base flows, the pressure on a two-dimensional base cannot be predicted accurately because of the imperfectly understood influence of the approach boundary layer (the boundary layer on the surface ahead of the base). When therefore, values of two-dimensional base pressure were required to provide a datum in the analysis of other experiments, some tests on two-dimensional steps were made. These tests are recorded here.

To further the understanding of base flows in general, the scope of the experiment was widened to include: firstly large changes in the ratio of the step height to the thickness of the approach boundary layer; secondly measurements of the pressure recovery downstream of the steps; and lastly a limited examination of the flow field downstream of one step.

2. *Description of Wind Tunnel and Models.*

The tests were made in the Royal Aircraft Establishment No. 2 supersonic, continuous-flow tunnel of $5\frac{1}{2}$ in. $\times$ $5\frac{3}{4}$ in. working cross-section. Dry air at a total pressure of 1 atmosphere and a total temperature of 20°C is drawn through this tunnel by suction pumps.

Two models were used. Each was mounted so that its top face formed a continuation, in the free-stream direction, of the lower liner of the tunnel. The top face of each model terminated at a step down to a floor plate aligned with the free stream.

Fig. 1 shows model No. 1 which enabled the height of the backward-facing step to be increased from zero to approximately 0·1 in. by inserting thin spacers under the top plate of the model. As it was not practicable to measure the pressure on the step face, the step was undercut to enable the leading static-pressure hole in the floor plate to lie under the top edge of the step. This static-pressure hole was as close as possible to the chamfer of the floor plate.

Model No. 2, shown in Fig. 2, provided steps of 0·2 in. and 0·8 in. in height. These steps were formed by blocks mounted on another floor plate fitted with a row of static-pressure holes along its centre-line. One end of each block was chamfered so that either right-angled or undercut steps could be tested by reversing the blocks. A base-pressure hole was drilled into each step face of each block.

In setting up the experiment, care was taken to avoid leaks at the steps of the models because base pressure changes rapidly when small quantities of air are bled into the flow behind a base. To ensure an undisturbed approach boundary layer, the gap between each model and the lower liner of the tunnel was sealed with modelling clay.

3. *Details of Tests.*

The tests were made at nominal Mach numbers of 1·56, 2·41 and 3·24. In each case the static pressures on the models were measured using mercury manometers. The manometers were referred to atmospheric pressure at $M = 1{\cdot}56$ and $2{\cdot}41$, but to vacuum at $M = 3{\cdot}24$. At this last Mach number, some of the pressures were also measured using di-butyl phthalate manometers referred to vacuum, and again using a McLeod gauge. Comparison of the methods of measurement showed that the mercury manometers, which were the most convenient to use, could be read with sufficient accuracy for the present study.

Micrometer pitot traverses of the boundary layers on the flat-plate extension of the top liner were made at each test Mach number. The traverse position was on the centre-line of the plate, 6 in. downstream of the end of the liner, at a point where there was a static-pressure hole in the plate. It was assumed, because of the symmetry of the working section, that these boundary layers (reduced slightly in thickness because the steps were 0·45 in. further upstream than the traverse station) would be the same as the approach boundary layers ahead of the steps.

The above measurements were made on the top liner because a traverse gear suitable for direct measurement of the step boundary layers was not available when the measurements were required. Later when suitable gear became available, it was used only to study the flow downstream of the step of height 0·8 in. at $M = 2{\cdot}41$, direct measurements on the approach boundary layers being thought unnecessary after examination of the earlier results.

An attempt was made to measure the static-pressure distribution downstream of the 0·8 in. step at M = 2·41. Because of the difficulty in aligning a static-pressure probe with the local stream direction a different technique was adopted: a reflection plate containing three rows of static-pressure orifices was mounted on model No. 2 as shown in Fig. 3a. Relevant dimensions of the reflection plate are shown in Fig. 3b.

At all Mach numbers, the measurements were supplemented by schlieren photographs taken with 0·01 second exposure to a continuous light source. In addition oil-flow patterns were made on model No. 2, using a light oil (OM 13) with which titanium dioxide pigment and a little oleic acid had been mixed.

4. *Presentation of Results.*

4.1. *Main-Stream Reference Conditions.*

4.1.1. *Static pressure and Mach number.*—The uniform pressure (p_w) downstream of the disturbances caused by step was chosen as that to which all other pressures should be referred. This choice was made for two reasons. Firstly, the work of Beastall and Eggink[1] and others has shown the importance of p_w in determining base pressures. Secondly, when steps of different sizes are compared, the use of this datum reduces the effect of slight departures from uniformity in the free stream. It was assumed that p_w was the static pressure at a point 12 step heights downstream of each step.

The corresponding Mach numbers (M_w) were taken to be those isentropically associated with p_w and the total pressure measured upstream of the nozzle liners. At the two lower test Mach numbers, the mean values of M_w equalled the liner design values of 1·56 and 2·41. In contrast, at the highest test Mach number the mean M_w was 3·10, although the liners were designed for $M = 3{\cdot}24$. This discrepancy does not imply an appreciable total pressure loss through the compressions behind the steps, because the approach boundary-layer traverse also indicated a low-tunnel Mach number (*see* Table 1).

4.1.2. *Boundary layers ahead of steps.*—The turbulent boundary layers ahead of the steps were assumed to have the characteristics given in Table 1. This table actually shows values derived from traverses of the boundary layers on the extension to the top liner block (*see* Section 3).

While the basic reason for using these measurements is the symmetry of the working section, it is felt that the case for accepting them is strengthened by the fact that they agreed closely at $M = 1{\cdot}56$ and $3{\cdot}10$ with simple estimates made in designing the experiment. At $M = 2{\cdot}41$, the measured boundary layer was thinner than had been expected but this experimental value was confirmed by a previous measurement[1] made on the lower liner.

4.2. *Pressure Measurements.*

4.2.1. *Floor static-pressure distributions.*—The floor static-pressure distributions are shown in Figs. 4, 5 and 6, from which it will be seen that not only are all the distributions similar in shape, but also that the rise occurs at similar positions when expressed in step heights. A comparison included in each figure, of results from an undercut and a right-angled step shows that the difference in step geometry has no significant effect on the floor pressures.

4.2.2. *Base pressures.*—Tests of the two types of step using model No. 2 and a step height of $0{\cdot}8$ in. showed that the differences between the three base pressures (two on the step face, and one on the floor at the foot of the step) were always within experimental error. For model No. 1 where no direct base-pressure measurement was possible, the base pressures recorded in Table 2 have therefore been taken from the floor pressure-distribution curves at points immediately below the top edges of the steps.

4.3. *Flow Visualisation.*

4.3.1. *Schlieren photographs.*—Although all the flows were observed by the schlieren method, only the set of photographs (Fig. 7) for $M_w = 2{\cdot}41$ is presented because the differences between this set and the photographs at $M_w = 1{\cdot}56$ and $3{\cdot}10$ are attributable solely to the different Mach angles.

Fig. 7 shows the flows behind steps ranging in height from $0{\cdot}032$ in. to $0{\cdot}8$ in. Because the floor pressure distributions suggest that the flows should possess some similarity when step height is the unit of length, the pictures in Fig. 7 are as far as possible to the same scale in this unit. It is apparent that when the whole base flow is embedded in the boundary layer as in Fig. 7a it is not very different from the much larger-scale flow (in Fig. 7h) which appears completely to absorb the approach boundary layer.

Fig. 7i shows that the flow pattern is not perceptibly altered by the change to a right-angled step from the undercut step of Fig. 7h.

4.3.2. *Oil-flow patterns.*—A few oil-flow patterns were made on model No. 2; model No. 1 was not used because of the danger of permanently blocking its small static-pressure holes. The results, which are consequently restricted to step heights of $0{\cdot}2$ and $0{\cdot}8$ in. are shown in Fig. 8.

The series 8a, b and c show that the primary re-attachment band (R) is closest to the step at the highest Mach number and shifts downstream progressively when the Mach number is lowered. At some 40% of the distance between the step and the re-attachment band the reverse flow is thought to separate from the floor plate at S. The ridge at S, most clearly visible on Figs. 8a and d, is considered to mark the meeting point of the reverse flow and a secondary flow from the step towards S. The free end of a silk thread, cemented at the other end to the floor plate near S was

observed to rise well clear of the floor and to oscillate. Similar threads cemented to the floor close to, and on either side of, the band R were observed to trail flat on the floor plate in opposite directions.

The oil-flow patterns 8a, b and c also show some bending of the streamlines at distances more than one step height or so from the centre-line of the model and the occurrence of corner vortices, with axes normal to the floor, where the step flow interacts with the sidewall boundary layer. These evidences of three-dimensional flow over part of the span cast some doubt on the assumption, made in the later discussion of the base pressures, that the measurements made on the centre-line of the large step are truly representative of two-dimensional flow.

Figs. 8d and e show that for step heights of 0·2 in. (and therefore for smaller steps) two-dimensional flow on the centre-line may reasonably be assumed.

These two pictures also enable the patterns from right-angled and undercut steps to be compared. The much better defined re-attachment line in (d) than in (e) arises more probably from some slight difference in oil-pigment mixture on model surface condition than from any difference between the airflows yielding the patterns.

4.4. *Flow Field behind a Step.*

The flow field behind the right-angled, 0·8 in. step was examined at $M_w = 2{\cdot}41$. The results are shown in Figs. 9, 10 and 11.

In addition to information available from the work already described, Fig. 9 contains, at (a), an idealised isobar pattern drawn by making the following assumptions:

(1) constant pressure on normals to the floor plate up to a displacement surface[2] which is a stream surface in inviscid flow,

(2) simple wave flow above that displacement surface.

These assumptions in conjunction with the floor static-pressure distribution shown in Fig. 9b enable the shape of the displacement surface to be derived as follows. By assumption (1), the pressure distribution on the displacement surface is obtained directly from the floor pressure distribution. By assumption (2), the pressure at any point on the displacement surface is related to the angle between the stream at that point and some reference direction. Since the pressure is p_w when the flow is parallel to the floor plate the flow direction relative to the floor plate, and thus the slope of the displacement surface, can be found. Integration of this slope gives the shape of the displacement surface. Its position is fixed by making it continuous with the displacement thickness of the approach boundary layer at a point chosen to match the leading edge of the expansion fan (outside the boundary layer) to the schlieren photograph.

Since for x/h greater than about 0·5 the displacement surface is concave upwards, isobars above it converge and eventually intersect. In the diagram of Fig. 9a that part of each isobar downstream of its first intersection with another isobar representing a higher pressure has been suppressed. The locus of such intersections of isobars (which by assumption (2) are characteristics) agrees very well with the trailing shock wave shown by schlieren. Although simple wave flow no longer exists once the isobars have intersected, it remains a good approximation to assume that behind a weak shock wave the isobars are the straight characteristics originating at the displacement surface downstream of the shock wave[3].

Fig. 10a, b, c shows a quantitative comparison of static-pressure profiles obtained from Fig. 9a with experimental data.

Direct measurements of static pressure were made with the reflection-plate arrangement shown in Fig. 3. These measurements follow the computed profiles quite closely at $x/h = 0{\cdot}75$ (Fig. 10a) and $x/h = 2{\cdot}5$ (Fig. 10b), except that in the latter case the sharp corner in the computed profile is, as one might expect, replaced by a smooth curve in the real flow.

At $x/h = 5{\cdot}5$, (Fig. 10c) the measured pressures deviate from the computed profiles for heights $0{\cdot}5 < z/h < 1{\cdot}5$. The deviations are thought to be associated with boundary-layer separation on the reflection plate. An oil-flow pattern showing such a separation on the reflection plate is given in Fig. 12. Fig. 13 shows the slight alteration in the floor pressure distribution produced by fitting this plate.

Static pressures deduced from a series of pitot traverses are also shown in Fig. 10. These static pressures were computed by assuming that there was free-stream total pressure ahead of the pitot shock-wave; they therefore deviate from the true static pressures where this assumption is not true, i.e. for small z where the pitot was in the shear layer. At $x/h = 2{\cdot}5$ and $5{\cdot}5$, and small z, the total pressure may have been further reduced because the pitot was behind the trailing compression. The compression was, however, spread over so great a length that it was probably very nearly isentropic. It will be seen that, except for small z, this set of static pressures is generally in good agreement with the others. At $x/h = 2{\cdot}5$ (Fig. 10b) the deduced static-pressure distribution is somewhat irregular. The reason is believed to be that the pitot sensed the weak shock (often called the 'lip' shock) which sprang from the top of the step just behind the expansion fan, and which was ignored in constructing the idealised isobar pattern.

Although Fig. 10 gives a good qualitative picture of the static pressures behind the step, it does not provide numerical values accurate enough for the derivation of shear-layer velocity profiles from the pitot traverses. Consequently no further analysis of the pitot-pressure profiles has been attempted. The measurements themselves are presented in Fig. 11.

5. *Analysis of Base-Pressure Measurements.*

5.1. *General Considerations.*

On dimensional grounds, a base pressure ratio might be expected to depend on the Mach number, the Reynolds number, and the ratio of the supposedly significant lengths—step height and some boundary-layer thickness. When the ratio of boundary-layer thickness to step height becomes zero, an approximate analysis given by Korst[4] gives ratios of base pressure to free-stream static pressure which are a function of Mach number only. This function is shown in Fig. 14 where it is compared with some values extrapolated from experiment, and others derived* from an empirical relation:

$$\frac{p_w}{p_b} = 1 + \frac{M_1^2}{4} \tag{1}$$

where M_1 = Mach number in the main stream when the static pressure is p_b.

Equation (1) was given by Beastall and Eggink[1] for bases with thin approach boundary layers. It will be seen that the theory is closely followed both by the experimental results and the deduction from equation (1).

---

* Isentropic compression from p_b to p_w was assumed in deriving M_w from M_1 to yield the base-pressure ratio in terms of M_w, which then equals the Mach number M_∞ of the undisturbed stream. Compression by a single oblique shock would lead to rather lower base pressures at Mach numbers (M_∞) above $2{\cdot}5$.

In order to assess the effects of finite approach boundary-layer thickness, Chapman[5] proposed that base-pressure ratios should be correlated on the basis of the ratio of some boundary-layer thickness to step height. Such correlations have usually been found to yield the somewhat unsatisfactory results exemplified by Fig. 15 from which no general law could be deduced. An alternative approach to the estimation of base pressures is explored in the next section. Later, in Section 5.4, the implications of this approach are compared with some results of methods stemming more directly from Korst's work.

5.2. *A New Method of Correlation.*

Equation (1), though purely empirical, not only follows the trend of the more elaborate theory and experimental results, but may be given a tentative physical interpretation. If (1) is re-expressed in the form:

$$p_w - p_b = \frac{1}{4\gamma}\rho_1 u_1^2, \tag{2}$$

(where ρ_1 and u_1 are respectively the density and velocity in the main stream when the Mach number is M_1) it shows that the pressure rise behind the step is proportional to the rate of momentum flux in the main stream ahead of the compression. Since it is from this portion of the main stream that fluid is entrained as the mixing 'wedge' grows from the top edge of the step, the direct connection between the rate of momentum flux $\rho_1 u_1^2$ and the downstream rise in pressure from p_b to p_w seems plausible. Correlation is therefore attempted in terms of a pressure-recovery coefficient, C_p', defined by

$$C_p' = \frac{(p_w - p_b)}{\frac{1}{2}\rho_1 u_1^2} = \frac{\dfrac{p_w}{p_b} - 1}{0{\cdot}7M_1^2} \text{ for } \gamma = 1{\cdot}4. \tag{3}$$

As the ratio of boundary-layer thickness to step height increases, C_p' may be expected to fall for the following reason: since the length, relative to step height, of the downstream mixing region is substantially unaffected by increase of boundary-layer thickness, this increase causes a corresponding rise in the proportion of boundary layer in the fluid entrained from outside, and reduces the capacity of the mixing-region fluid to negotiate the trailing compression.

The values of C_p' for the present experiments, plotted against ϑ_a/h in Fig. 16a, form a simple family with M_w as a parameter. It appears that as the step height rises, C_p' approaches a limiting value of about 0·4.

As shown in Fig. 16b, a different independent variable, $v_s/u_\tau h$, considerably reduces the dependence of C_p' on M_w for the largest steps. The quantity u_τ is defined as $(\tau_s/\rho_s)^{1/2}$, where τ_s and ρ_s are the frictional stress and air density at the wall just ahead of the step. The kinematic viscosity v_s is evaluated at wall temperature.

In order to correlate the results for smaller steps, Preston's concept[6] of limited dynamical similarity was invoked. As applied to compressible flow[7], it implies that for geometrically-similar steps very much smaller than the boundary-layer thickness, dynamical similarity in terms of the variables τ_s, ρ_s, v_s, h may be expected. In particular, as in Ref. 7,

$$\frac{C_p}{c_{fa}} = f_1\left(\frac{hu_\tau}{v_s}\right),$$

where

$$C_p = \frac{p_b/p_a - 1}{\frac{\gamma}{2} M_a^2},$$

and

$$c_{fa} = \frac{\tau_s}{\frac{\gamma}{2} p_a M_a^2}.$$

For small steps (if the afterbody angle is small) the pressures p_a, p_w, p_b are nearly equal, M_1 is close to M_a, so that

$$\frac{C_p'}{c_{fa}} = f_2\left(\frac{hu_\tau}{v_s}\right).$$

Fig. 17 shows that the present results correlate fairly well on this basis. As for forward-facing steps[7], the correlation remains useful for remarkably large steps. There is, indeed, a possibility that C_p'/c_{fa} rather than C_p' itself tends to a limit as hu_τ/v_s tends to infinity.

5.3. *Comparison with Other Experiments.*

There are few base-pressure experiments for which the approach boundary-layer characteristics are either known or may confidently be estimated. The most extensive of these experiments are reported in Ref. 8. They were made on constant-chord wings, each having a basically diamond cross-section cut off at the trailing edge to form a base. A turbulent approach boundary layer was ensured by a roughness band on each wing. The base pressures are shown in Fig. 18. Some of their scatter may reasonably be ascribed to the effects of the different roughness bands and section proportions on the approach boundary layers.

Curves derived, where necessary by cross-plotting against M_w, from Fig. 16 are also shown in Fig. 18. The results from Ref. 8 support the contention that there is a limiting C_p' of about 0·4, but at the lower Mach numbers this limit is approached more rapidly than in the tests reported here.

Fig. 18d shows that most of the base pressures for these wings, when plotted as C_p'/c_{fa} against hu_τ/v_s, fall within the band containing the present test results. It is noteworthy that exceptions occur only when hu_τ/v_s is large.

Results from other experiments[1, 8, 9, 10] on steps have been examined. In all cases hu_τ/v_s was greater than 300. All showed a tendency for C_p' to approach a limit near 0·4, usually however more slowly than the present results.

It is tentatively concluded that there is a genuine limit:

$$C_p' \to 0{\cdot}40 \text{ approximately, as } \frac{hu_\tau}{v_s} \to \infty, \text{ for } 1{\cdot}5 \leqslant M_w \leqslant 3{\cdot}1.$$

Since for a wide range of hu_τ/v_s, C_p'/c_{fa} is approximately a function of hu_τ/v_s, the way in which this limit is approached may well depend on c_{fa}.

Although for $hu_\tau/v_s > 1000$ all results examined give values of C_p'/c_{fa} lying between 118 and 175, this is thought to reflect rather the narrow range of c_{fa} and a nearly constant C_p' than the existence of a limit for C_p'/c_{fa}.

It is worth noting that the non-linear relation between C_p' and the conventional base-pressure coefficient C_{pb} is such that, for large steps, errors in C_{pb} estimated using correlations of C_p' will be smaller than errors in the chosen C_p'. This behaviour is accentuated by increase of Mach number as shown by the comparison of the two coefficients in Fig. 19.

Coefficients similar to C_p' have been introduced in studies of other flow regions where pressure recovery is controlled by turbulent mixing. Two examples are quoted below.

Crabtree[11], investigating closed separation bubbles on thin aerofoils in low-speed flow, defined a coefficient (denoted by σ) for the pressure rise to re-attachment in the closing region of a bubble. He proposed a limiting value of about 0·35 for this parameter. Since re-attachment takes place near the top of the pressure rise associated with the presence of the bubble on a thin aerofoil, σ has much the same significance as C_p'. It remains somewhat surprising that the proposed limiting values of σ and C_p' are nearly equal, since the bubble on a thin aerofoil is bounded by a mixing region which is initially laminar, unlike the mixing regions behind the steps studied here.

In a discussion of the transonic drag of wings[12], the pressure recovery through a shock wave on an aerofoil was expressed in the same form and assigned rough values equivalent to C_p' equal to 1/3 or 1/2 for boundary layers respectively laminar or turbulent ahead of the shock wave.

5.4. *A Brief Comparison of Base-Pressure Predictions.*

Three papers 13, 14, 15 refining and extending Korst's analysis[4] have fairly recently appeared. They follow earlier work (which is thoroughly discussed by Nash[13]) in matching a computed mixing region to an inviscid outer flow. They improve the theory principally by more realistic treatments of the downstream re-attachment region.

Although differing from one another, their results have in common base-pressure ratios at $\theta_a/h = 0$, which are much lower than would correspond to $C_p' = 0{\cdot}4$. Implied values of C_p' range from about 0·70 to 0·83 and 0·55 to 0·84 at Mach numbers (M_∞) of 2 and 3. The possible effect of c_{fa} (or some equivalent parameter such as approach momentum thickness Reynolds number) on the approach to the (lowest) limiting base pressure does not emerge from these analyses. Such an effect, mentioned in Section 5.3, might explain the difference seen in Fig. 18 between the results of Ref. 8 and the present measurements.

6. *Conclusions.*

Studies of the flow fields downstream of two-dimensional, rearward-facing steps with turbulent approach boundary layers have shown that, in the Mach number range 1·56 to 3·10:

(*a*) measured in step heights, the streamwise extent of the disturbance caused by the step is independent of both Mach number and step size relative to approach boundary layer;

(*b*) in the region of dissipative flow downstream of a step there are pressure gradients along both normals and streamwise tangents to mean stream surfaces;

(*c*) the length occupied by the recompression downstream of a step is sufficient for the compression to be considered isentropic.

Some correlation of base pressures for a wide range of step heights is possible using the concept of local similarity based on the 'law of the wall' for turbulent boundary layers, in conjunction with a pressure-recovery coefficient for the flow downstream of a step. This coefficient apparently reaches a limiting value near 0·4 for steps much larger than the approach boundary-layer thickness.

LIST OF SYMBOLS

c_{fa}	Skin-friction coefficient just ahead of base or step
C_{pb}	Base-pressure coefficient $= \dfrac{p_b/p_\infty - 1}{0{\cdot}7M_\infty{}^2}$
$C_p{}'$	Pressure-recovery coefficient $= \dfrac{p_w/p_b - 1}{0{\cdot}7M_1{}^2}$
h	Step height ($= \frac{1}{2}$ base thickness)
M	Mach number
n	Distance outward from surface along pitot traverse
p	Static pressure
${}_pp$	Pitot pressure
${}_tp_\infty$	Total pressure of undisturbed stream
Re_h	Reynolds number based on undisturbed stream properties and step height
u	x-wise velocity component
u_τ	'Frictional velocity' just ahead of step $= \left(\dfrac{\tau_s}{\rho_s}\right)^{1/2}$
x	Co-ordinate downstream from top of step
z	Co-ordinate upward from foot of step
$\delta_a{}^*$	Displacement thickness of boundary layer just ahead of step
ϑ_a	Momentum thickness of boundary layer just ahead of step
v_s	Kinematic viscosity at wall temperature just ahead of step
ρ	Density of fluid
τ_s	Skin-frictional stress just ahead of step

Subscripts

Subscripts used solely in conjunction with a single symbol, and already defined, are omitted.

a	Conditions just ahead of base
b	Step face or base
s	Surface conditions, just ahead of step
w	Uniform conditions well downstream of step
1	Conditions in main stream where its static pressure is p_b
∞	Undisturbed stream conditions

REFERENCES

No.	*Author(s)*	*Title, etc.*
1	D. Beastall and H. Eggink ..	Some experiments on breakaway in supersonic flow (part II). Unpublished M.o.A. Report.
2	M. J. Lighthill	On displacement thickness. *J. Fluid Mech.*, Vol. 4, Part 4. August, 1958.
3	M. J. Lighthill	*General theory of high-speed aerodynamics.* W. R. Sears, editor. O.U.P., p. 379 et seq. 1955.
4	H. H. Korst	A theory for base pressures in transonic and supersonic flow. *J. App. Mech.*, Vol. 23, No. 4, pp. 593 to 600. December, 1956.
5	D. R. Chapman	An analysis of base pressure at supersonic velocities and comparison with experiments. N.A.C.A. Report 1051. 1951.
6	J. H. Preston	The determination of turbulent skin friction by means of pitot tubes. *J. R. Ae. Soc.*, Vol. 58, pp. 109 to 121. 1954.
7	K. G. Smith, L. Gaudet and K. G. Winter	The use of surface pitot tubes as skin-friction meters at supersonic speeds. A.R.C. R. & M. 3351. June, 1962.
8	D. R. Chapman, W. R. Wimbrow and R. H. Kester	Experimental investigation of base pressure on blunt-trailing-edge wings at supersonic velocities. N.A.C.A. Report 1109. 1952.
9	M. Sirieix	Pression de culot et processus de mélange turbulent en écoulement supersonique plan. *La Recherche Aéronautique*, No. 78, pp. 13 to 20. September/October, 1960.
10	L. Fuller and J. Reid	Experiments on two-dimensional base flow at $M = 2{\cdot}4$. A.R.C. R. & M. 3064. February, 1956.
11	L. F. Crabtree	The formation of regions of separated flow on wing surfaces. Part II: Laminar separation bubbles and the mechanism of the leading-edge stall. A.R.C. R. & M. 3122. July, 1957.
12	D. Küchemann	Methods of reducing the transonic drag of swept-back wings at zero lift. *J. R. Aero. Soc.*, Vol. 61, pp. 37 to 42. 1957.
13	J. F. Nash	An analysis of two-dimensional turbulent base flow, including the effect of the approaching boundary layer. A.R.C. R. & M. 3344. July, 1962.
14	H. McDonald	Turbulent shear layer re-attachment with special emphasis on the base pressure problem. English Electric Aviation Limited, Report Ae. 175, Issue 2. A.R.C. 24 771. August, 1963.
15	J. C. Cooke	Separated supersonic flow. A.R.C. 24 935. March, 1963.

TABLE 1

Approach Boundary-Layer Characteristics

(just ahead of the step)

$M_a = M_w$	10^{-5} Re/in.	δ_a^* (in.)	ϑ_a (in.)	$\frac{\delta_a^*}{\vartheta_a}$
1·56	3·75	0·0441	0·0180	2·46
2·41	2·65	0·0684	0·0177	3·87
3·10	1·85	0·1143	0·0198	5·78

TABLE 2

Summary of Base-Pressure Results

(taken from floor pressure-distribution curves at points immediately below top edges of steps in cases where no direct measurements were made)

$M_w = 1·56$

h (in.)	$\frac{p_b}{p_w}$
0·010	0·707
0·022	0·645
0·031	0·620
0·044	0·593
0·066	0·573
0·098	0·550
0·20	0·510
*0·20	0·510
*0·80	0·467

$M_w = 2·41$

h (in.)	$\frac{p_b}{p_w}$
0·010	0·694
0·016	0·671
0·021	0·649
0·032	0·536
0·050	0·451
0·066	0·455
0·081	0·438
0·105	0·380
0·20	0·310
0·80	0·255
*0·80	0·255

$M_w = 3·10$

h (in.)	$\frac{p_b}{p_w}$
0·026	0·660
0·041	0·608
0·058	0·530
0·085	0·510
0·20	0·310
*0·20	0·380
*0·80	0·175

* denotes right-angled step, all others being for undercut steps.

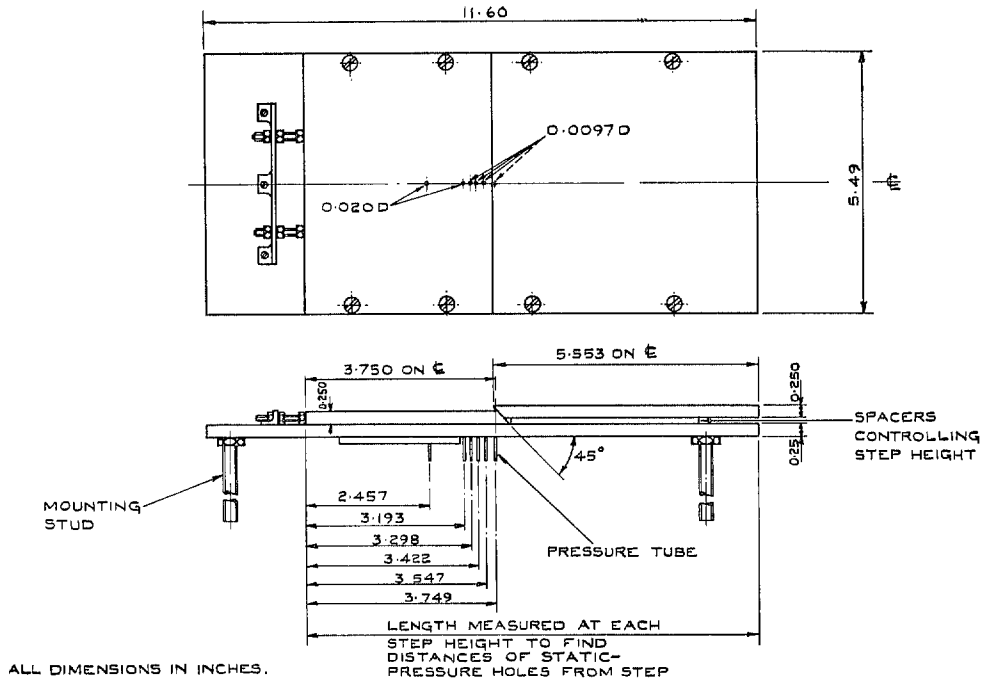

FIG. 1. Rearward-facing step model No. 1.

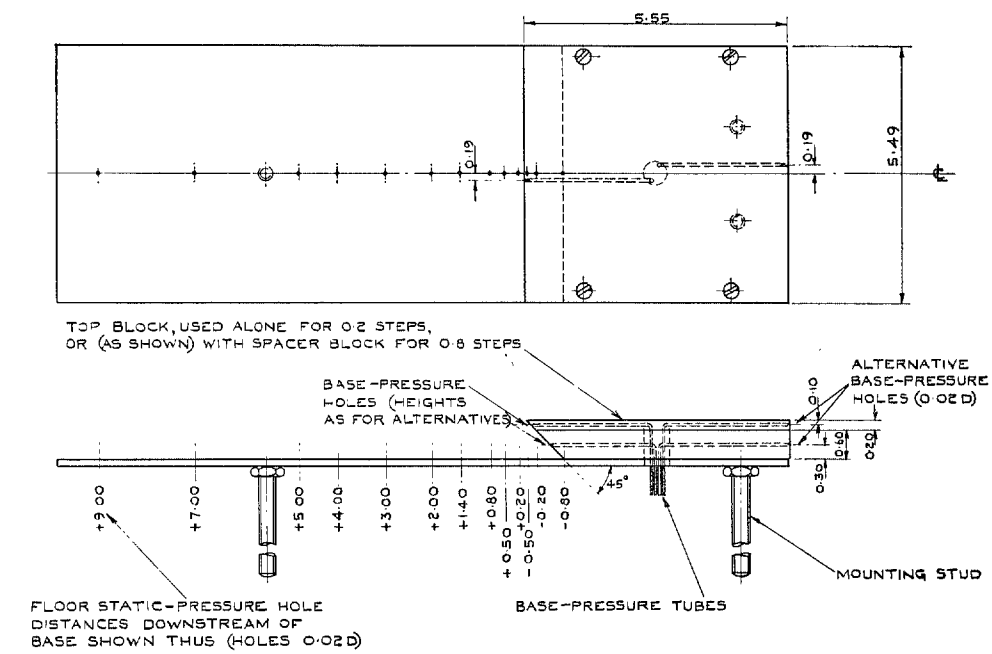

FIG. 2. Rearward-facing step model No. 2.

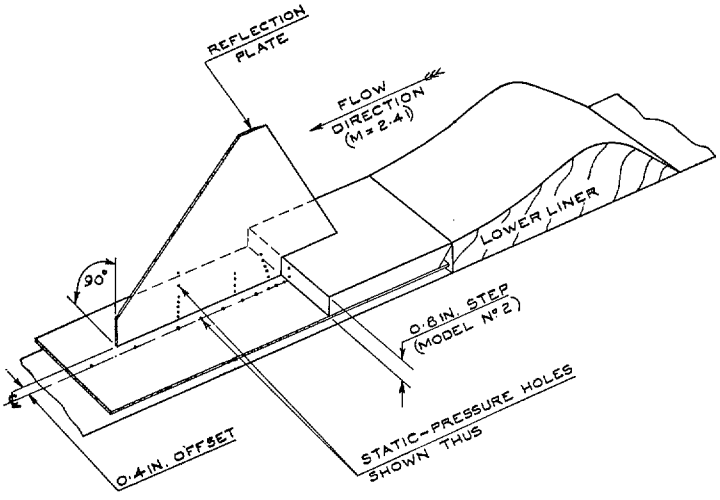

(a) DIAGRAM OF REFLECTION PLATE MOUNTED ON MODEL No. 2.

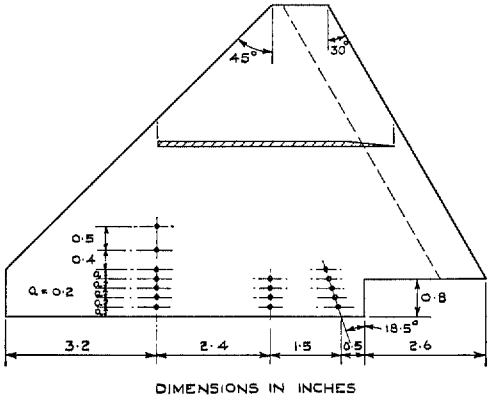

DIMENSIONS IN INCHES

(b) LEADING DIMENSIONS OF REFLECTION PLATE.

FIG. 3. Details of reflection plate.

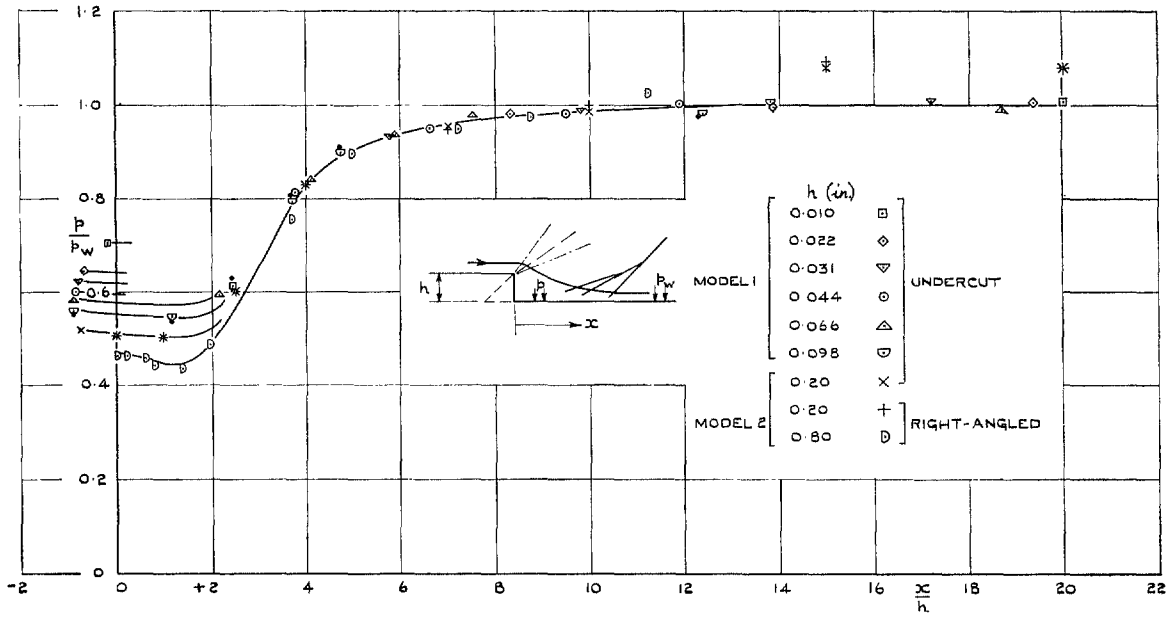

FIG. 4. Floor pressure distributions behind steps of various heights at a Mach number of 1·56.

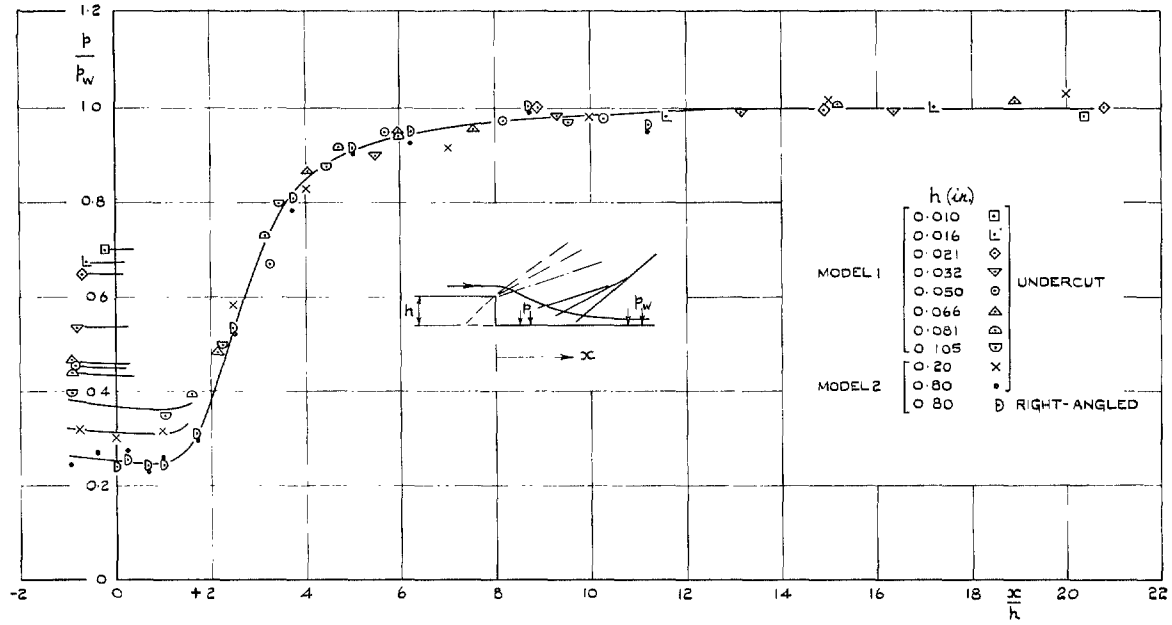

FIG. 5. Floor pressure distributions behind steps of various heights at a Mach number of 2·41.

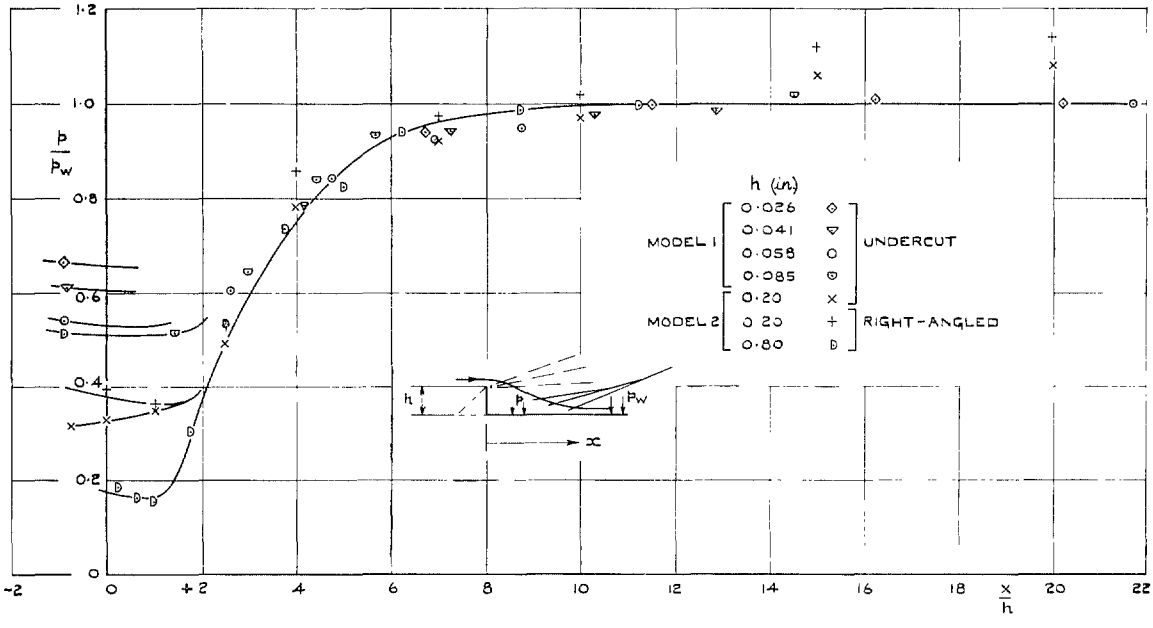

FIG. 6. Floor pressure distributions behind steps of various heights at a Mach number of 3·10.

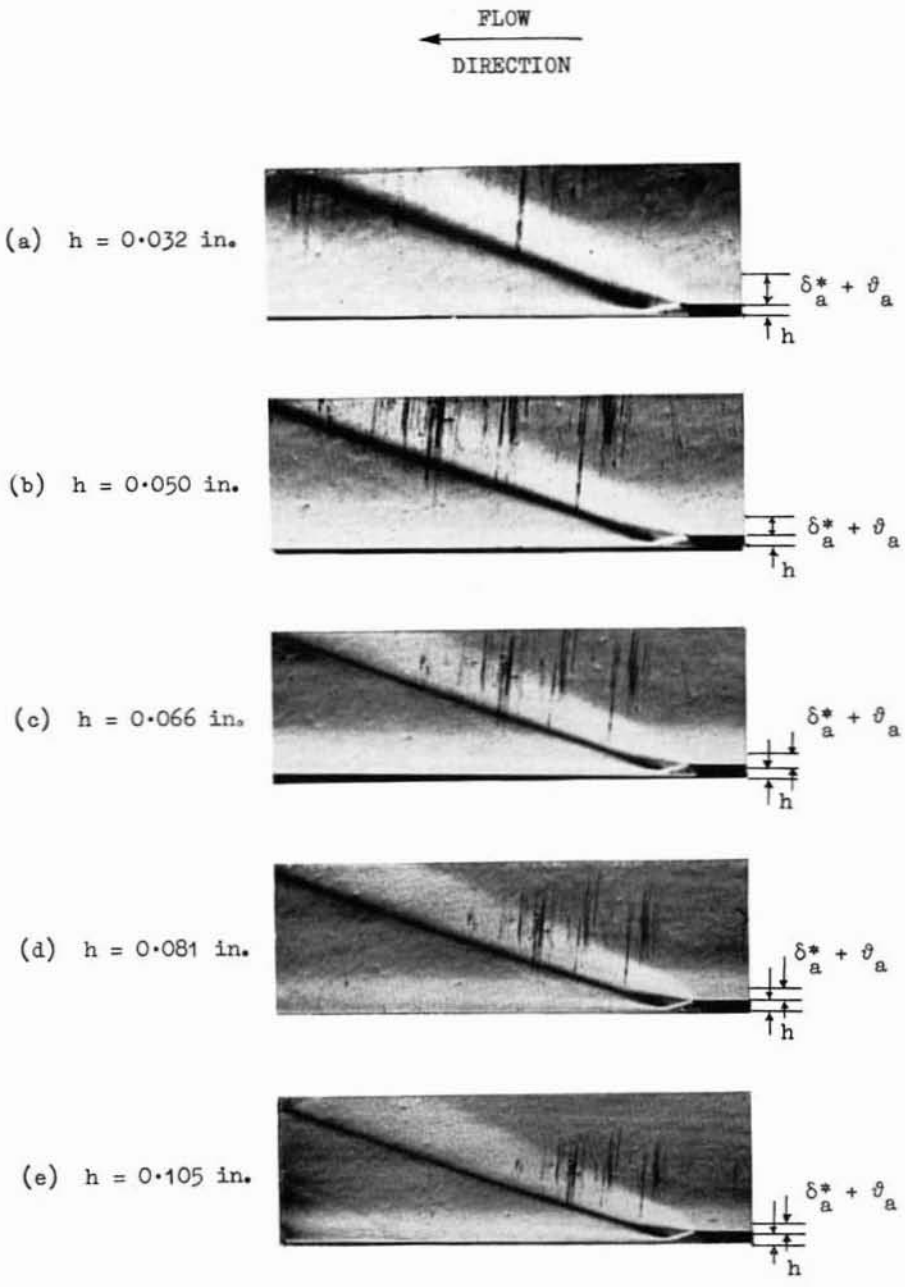

FIG. 7. Schlieren photographs of turbulent flow down steps;
$M_w = 2{\cdot}41$, $\delta_a^* = 0{\cdot}0684$ in., $\vartheta_a = 0{\cdot}0177$ in.

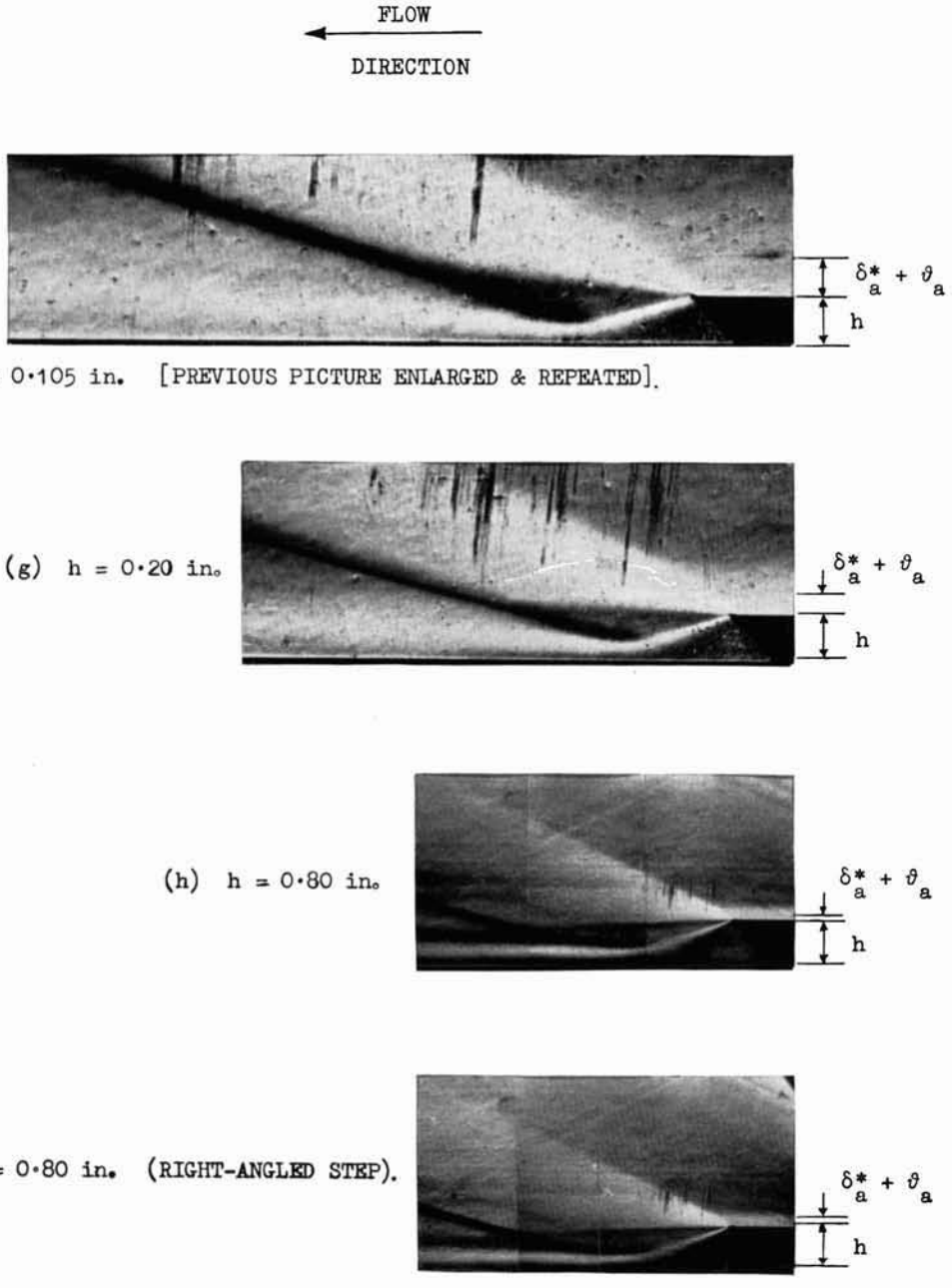

FIG. 7—*concluded.* Schlieren photographs of turbulent flow down steps;
$M_w = 2{\cdot}41$, $\delta_a{}^* = 0{\cdot}0684$ in., $\vartheta_a = 0{\cdot}0177$ in.

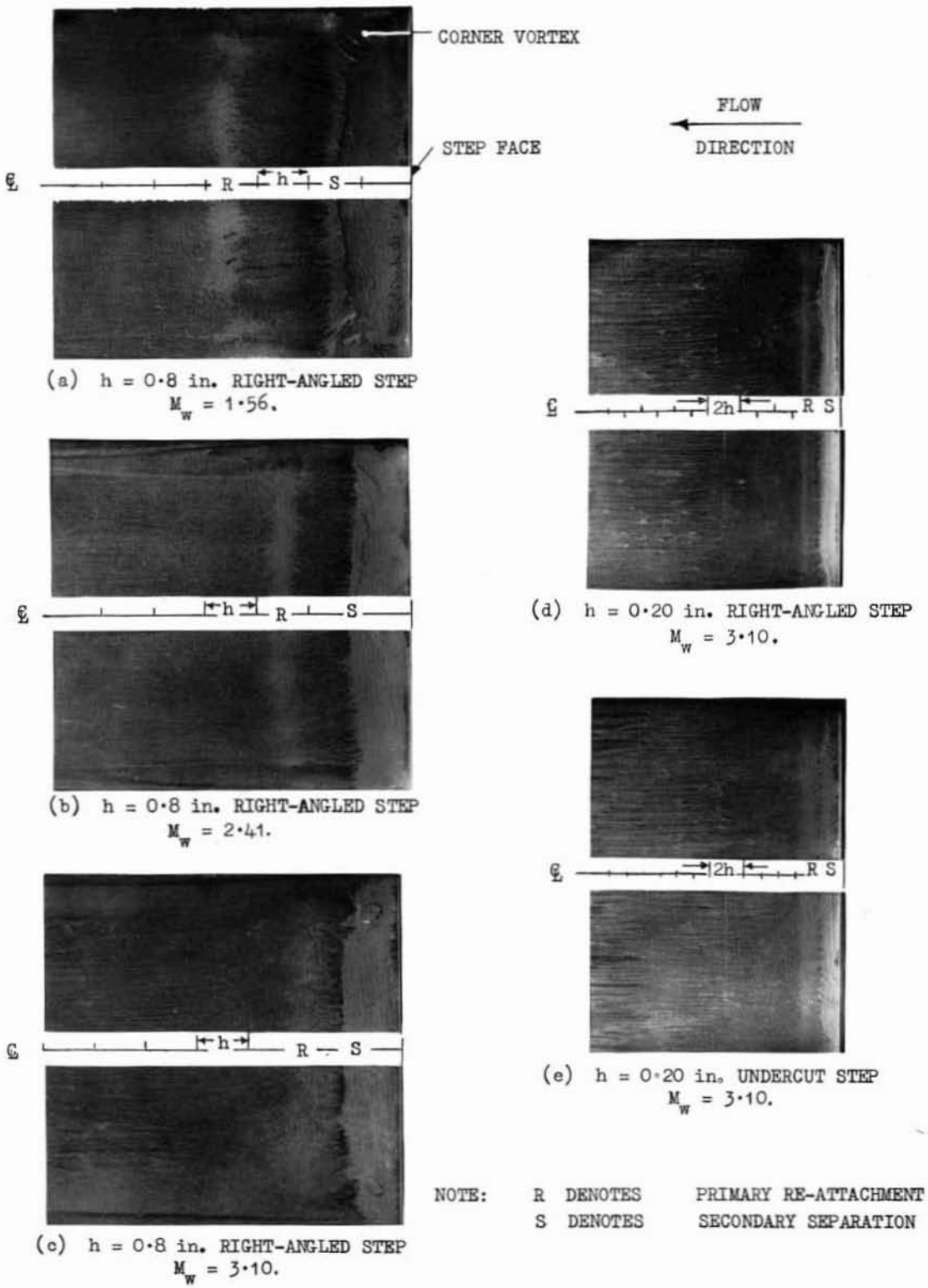

FIG. 8. Floor oil-flow patterns.

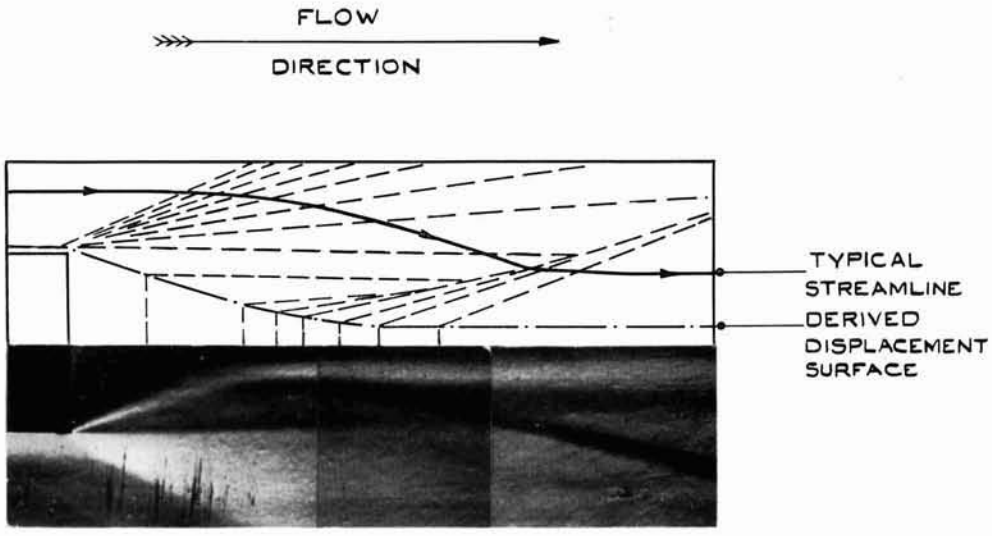

(a) IDEALISED ISOBAR PATTERN & SCHLIEREN PHOTOGRAPH.

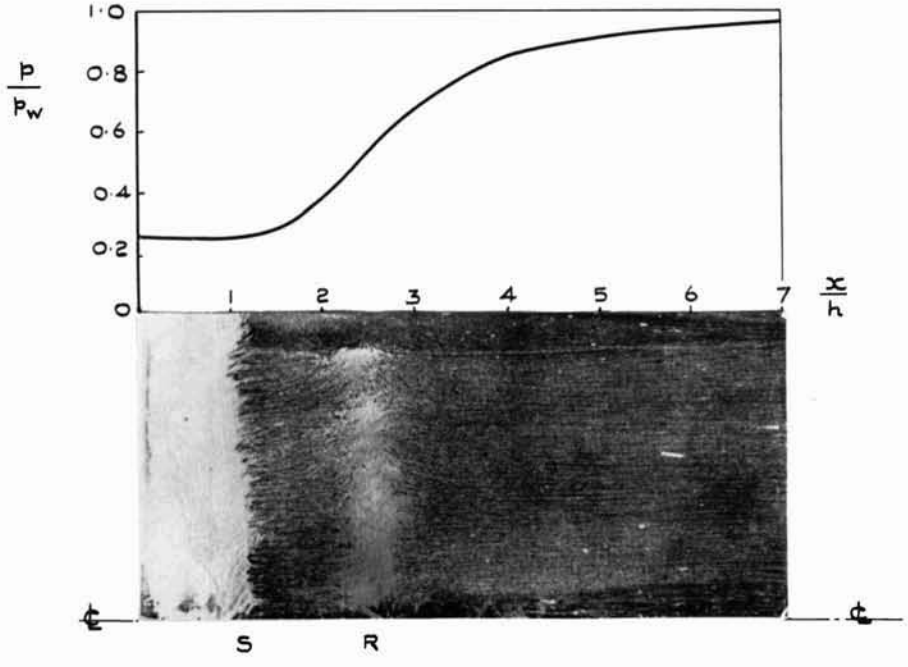

(b) FLOOR OIL-FLOW PATTERN & PRESSURE DISTRIBUTION.

FIG. 9. Main features of flow aft of step for $h = 0{\cdot}8$ in. and $M_w = 2{\cdot}41$.

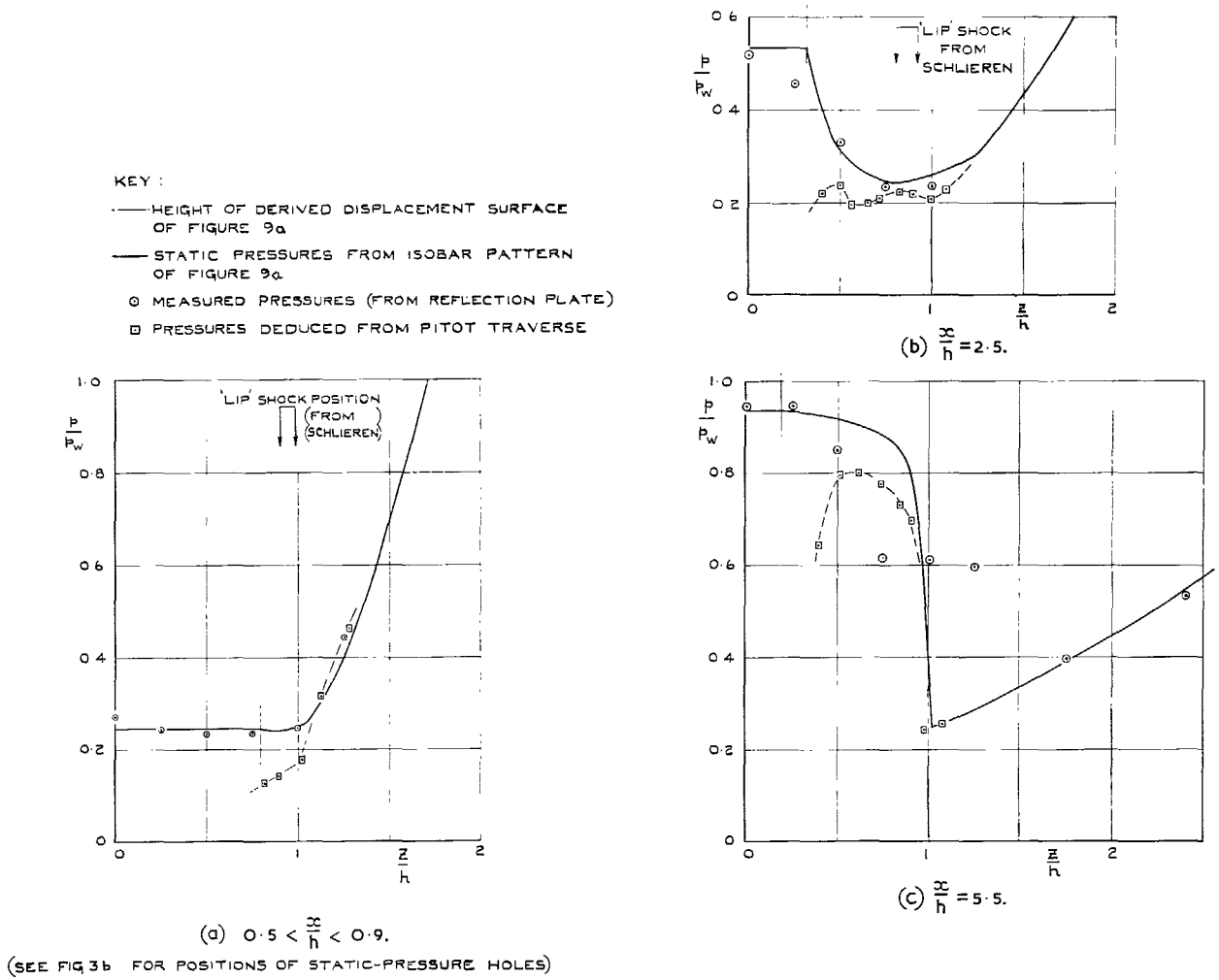

FIG. 10. Static-pressure profiles aft of step for $h = 0{\cdot}8$ in. and $M_w = 2{\cdot}41$.

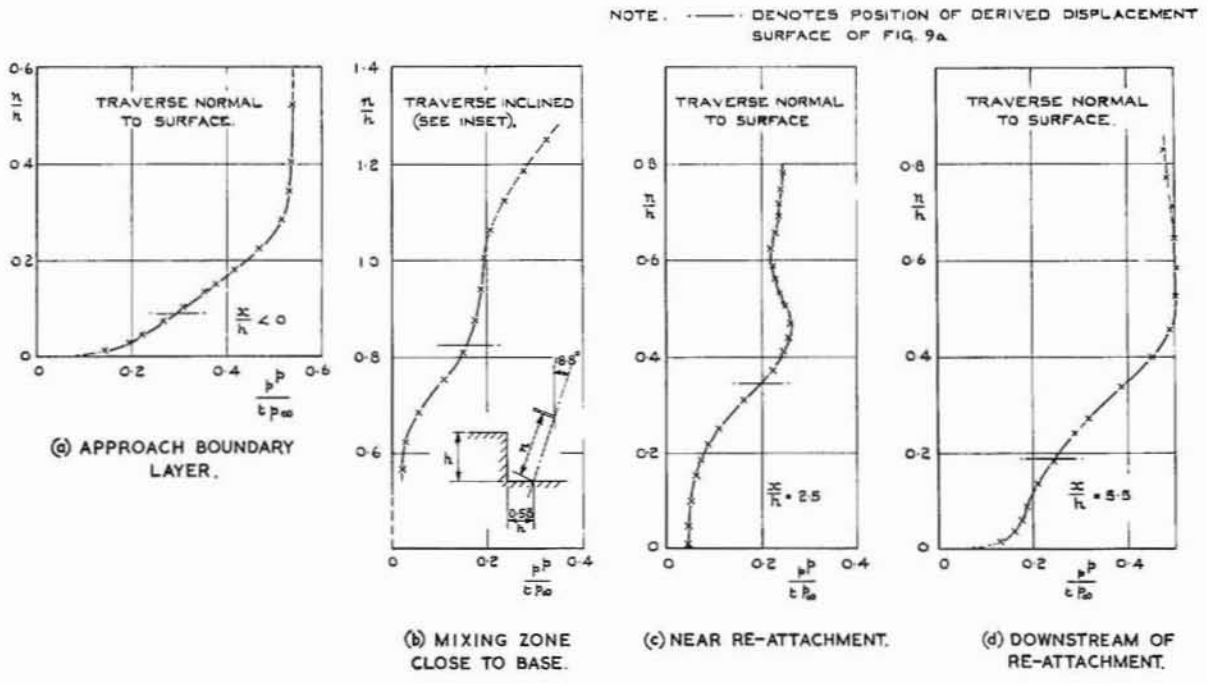

FIG. 11. Pitot-pressure profiles aft of step for $h = 0{\cdot}8$ in. and $M_w = 2{\cdot}41$.

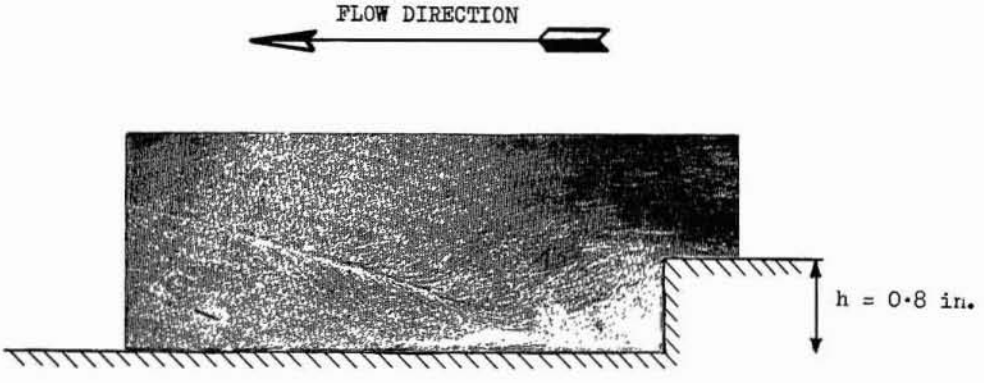

FIG. 12. Oil-flow pattern showing separation on reflection plate ($M_w = 2{\cdot}41$).

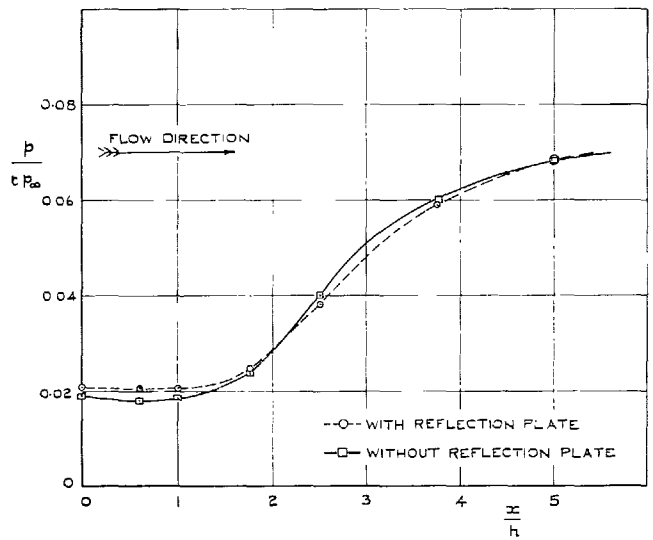

FIG. 13. Floor pressure distributions with and without reflection plate ($h = 0{\cdot}8$ in., $M_w = 2{\cdot}41$).

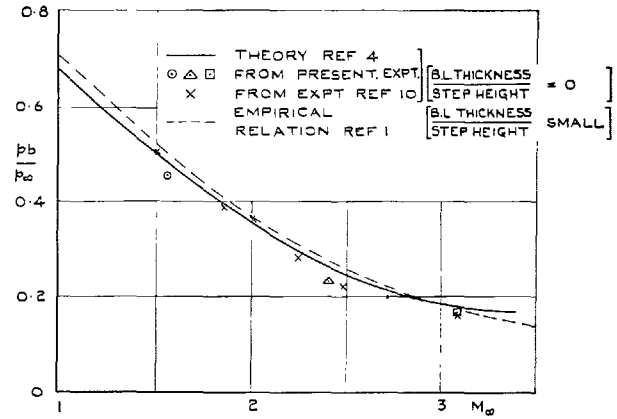

FIG. 14. Two-dimensional base-pressure ratios vs. Mach number for (boundary-layer thickness/step height) $\to 0$.

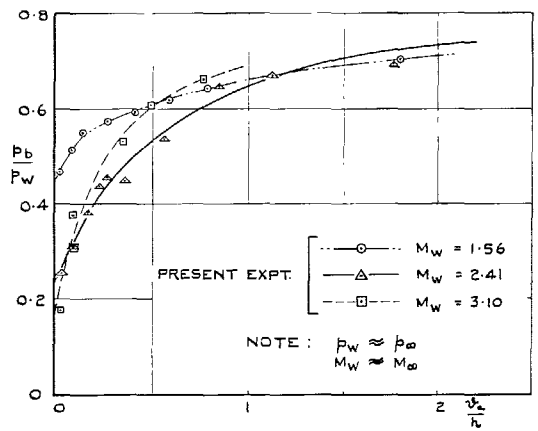

FIG. 15. Two-dimensional base-pressure ratios vs. (approach momentum thickness/step height) for the present tests.

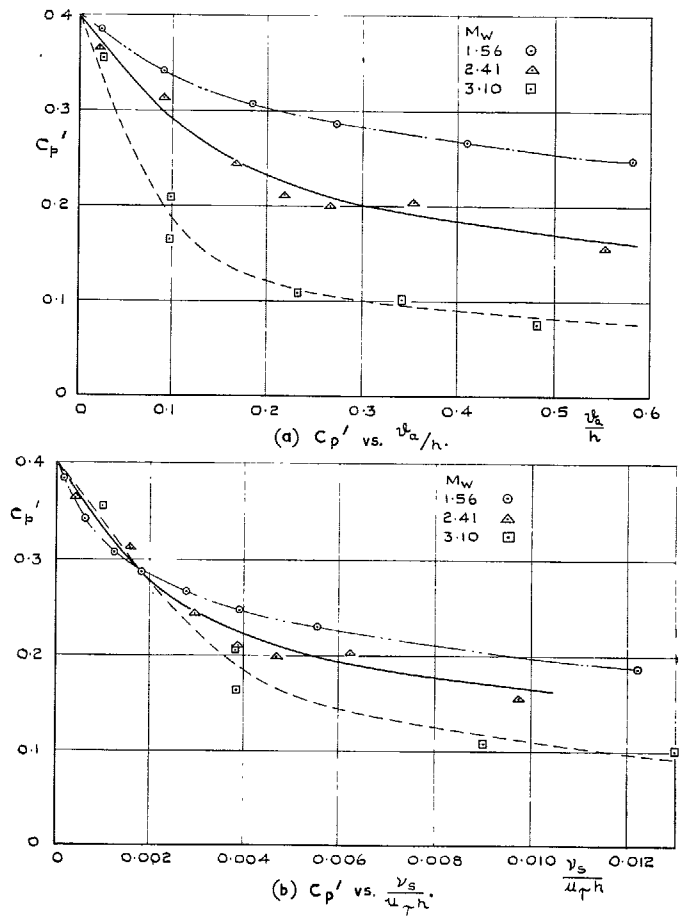

FIG. 16. Behaviour of the pressure-recovery coefficient C_p' for the larger steps of the present series.

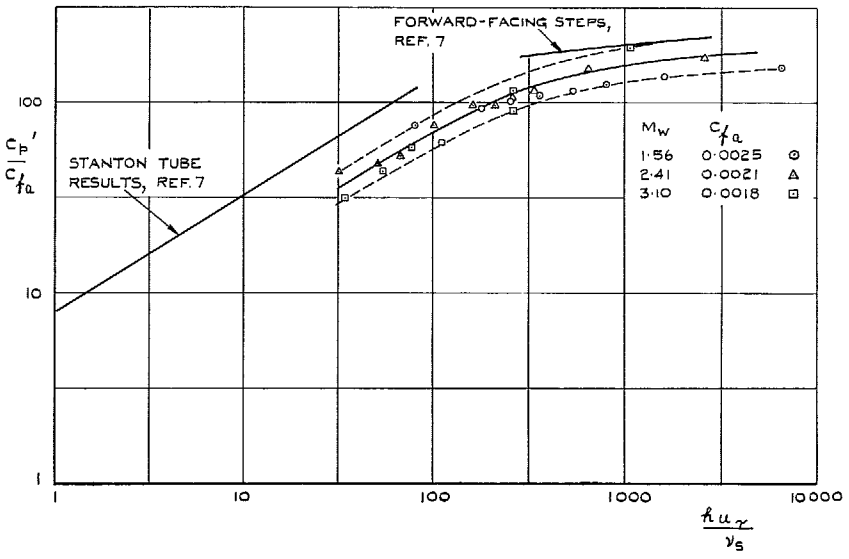

FIG. 17. Overall correlation of present results.

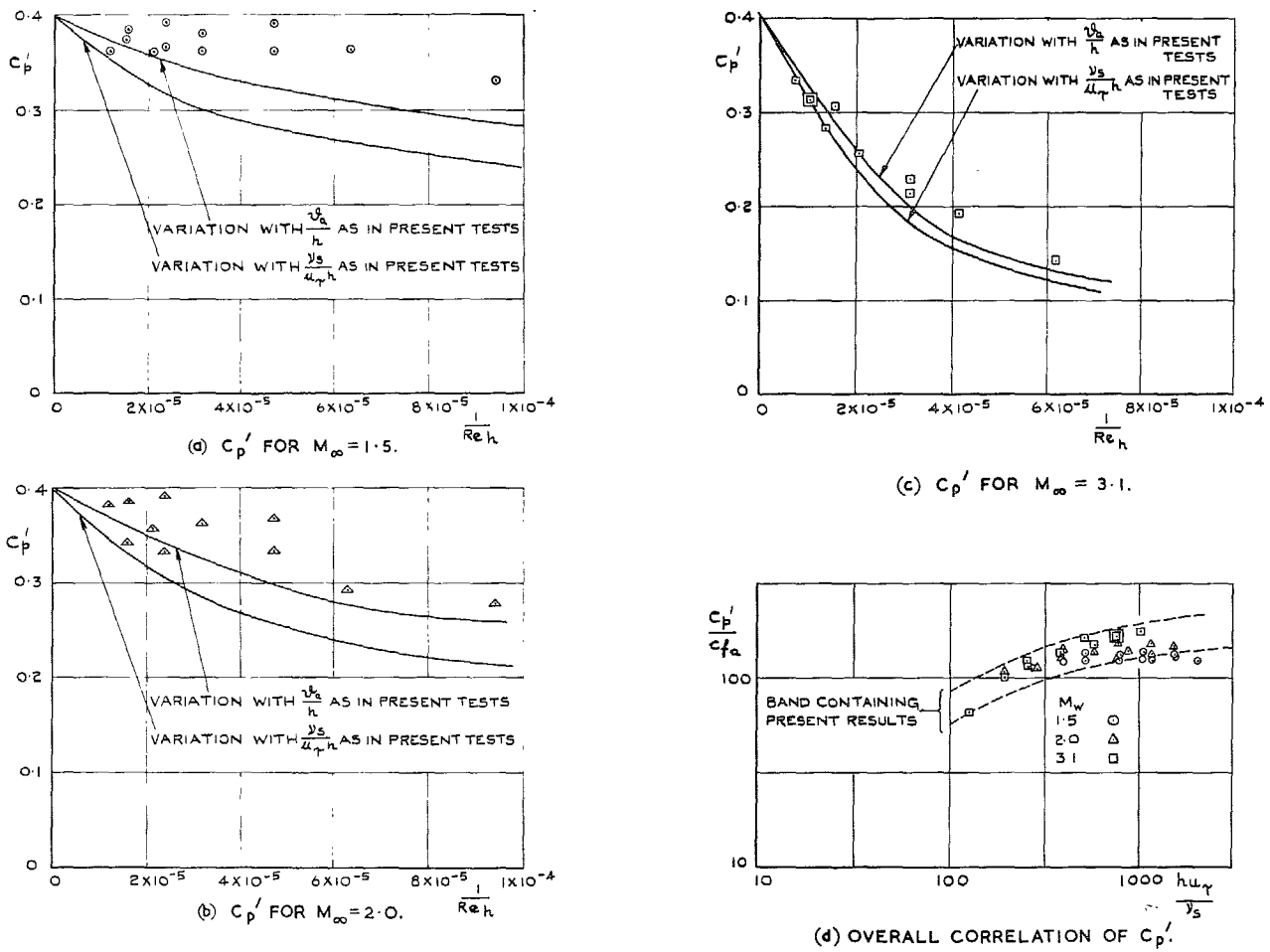

FIG. 18. Behaviour of pressure-recovery coefficients from Ref. 8.

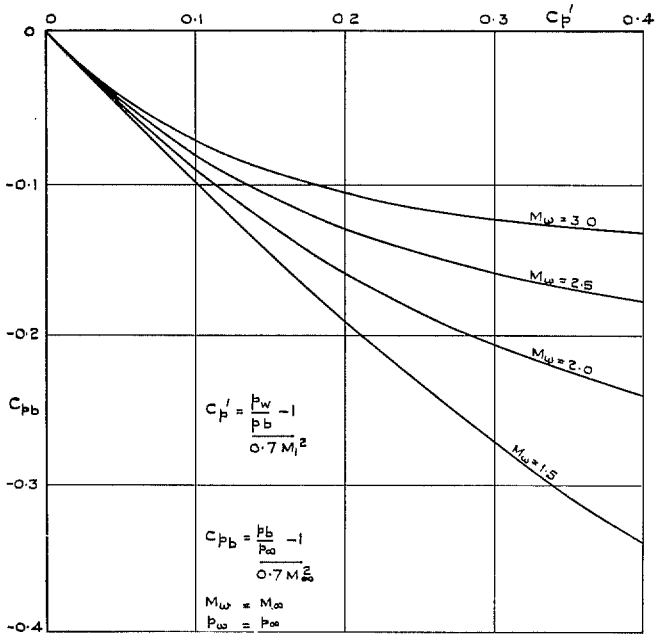

FIG. 19. Comparison of pressure-recovery and conventional base-pressure coefficients.

(90993) Wt. 66/2301 K 5 3/65 Hw.

Publications of the Aeronautical Research Council

ANNUAL TECHNICAL REPORTS OF THE AERONAUTICAL RESEARCH COUNCIL (BOUND VOLUMES)

1942 Vol. I. Aero and Hydrodynamics, Aerofoils, Airscrews, Engines. 75*s.* (post 2*s.* 9*d.*)
Vol. II. Noise, Parachutes, Stability and Control, Structures, Vibration, Wind Tunnels. 47*s.* 6*d.* (post 2*s.* 3*d.*)

1943 Vol. I. Aerodynamics, Aerofoils, Airscrews. 80*s.* (post 2*s.* 6*d.*)
Vol. II. Engines, Flutter, Materials, Parachutes, Performance, Stability and Control, Structures. 90*s.* (post 2*s.* 9*d.*)

1944 Vol. I. Aero and Hydrodynamics, Aerofoils, Aircraft, Airscrews, Controls. 84*s.* (post 3*s.*)
Vol. II. Flutter and Vibration, Materials, Miscellaneous, Navigation, Parachutes, Performance, Plates and Panels, Stability, Structures, Test Equipment, Wind Tunnels. 84*s.* (post 3*s.*)

1945 Vol. I. Aero and Hydrodynamics, Aerofoils. 130*s.* (post 3*s.* 6*d.*)
Vol. II. Aircraft, Airscrews, Controls. 130*s.* (post 3*s.* 6*d.*)
Vol. III. Flutter and Vibration, Instruments, Miscellaneous, Parachutes, Plates and Panels, Propulsion. 130*s.* (post 3*s.* 3*d.*)
Vol. IV. Stability, Structures, Wind Tunnels, Wind Tunnel Technique. 130*s.* (post 3*s.* 3*d.*)

1946 Vol. I. Accidents, Aerodynamics, Aerofoils and Hydrofoils. 168*s.* (post 3*s.* 9*d.*)
Vol. II. Airscrews, Cabin Cooling, Chemical Hazards, Controls, Flames, Flutter, Helicopters, Instruments and Instrumentation, Interference, Jets, Miscellaneous, Parachutes. 168*s.* (post 3*s.* 3*d.*)
Vol. III. Performance, Propulsion, Seaplanes, Stability, Structures, Wind Tunnels. 168*s.* (post 3*s.* 6*d.*)

1947 Vol. I. Aerodynamics, Aerofoils, Aircraft. 168*s.* (post 3*s.* 9*d.*)
Vol. II. Airscrews and Rotors, Controls, Flutter, Materials, Miscellaneous, Parachutes, Propulsion, Seaplanes, Stability, Structures, Take-off and Landing. 168*s.* (post 3*s.* 9*d.*)

1948 Vol. I. Aerodynamics, Aerofoils, Aircraft, Airscrews, Controls, Flutter and Vibration, Helicopters, Instruments, Propulsion, Seaplane, Stability, Structures, Wind Tunnels. 130*s.* (post 3*s.* 3*d.*)
Vol. II. Aerodynamics, Aerofoils, Aircraft, Airscrews, Controls, Flutter and Vibration, Helicopters, Instruments, Propulsion, Seaplane, Stability, Structures, Wind Tunnels. 110*s.* (post 3*s.* 3*d.*)

Special Volumes

Vol. I. Aero and Hydrodynamics, Aerofoils, Controls, Flutter, Kites, Parachutes, Performance, Propulsion, Stability. 126*s.* (post 3*s.*)
Vol. II. Aero and Hydrodynamics, Aerofoils, Airscrews, Controls, Flutter, Materials, Miscellaneous, Parachutes, Propulsion, Stability, Structures. 147*s.* (post 3*s.*)
Vol. III. Aero and Hydrodynamics, Aerofoils, Airscrews, Controls, Flutter, Kites, Miscellaneous, Parachutes, Propulsion, Seaplanes, Stability, Structures, Test Equipment. 189*s.* (post 3*s.* 9*d.*)

Reviews of the Aeronautical Research Council

1939–48 3*s.* (post 6*d.*) 1949–54 5*s.* (post 5*d.*)

Index to all Reports and Memoranda published in the Annual Technical Reports

1909–1947 R. & M. 2600 (out of print)

Indexes to the Reports and Memoranda of the Aeronautical Research Council

Between Nos. 2351–2449	R. & M. No. 2450 2*s.* (post 3*d.*)
Between Nos. 2451–2549	R. & M. No. 2550 2*s.* 6*d.* (post 3*d.*)
Between Nos. 2551–2649	R. & M. No. 2650 2*s.* 6*d.* (post 3*d.*)
Between Nos. 2651–2749	R. & M. No. 2750 2*s.* 6*d.* (post 3*d.*)
Between Nos. 2751–2849	R. & M. No. 2850 2*s.* 6*d.* (post 3*d.*)
Between Nos. 2851–2949	R. & M. No. 2950 3*s.* (post 3*d.*)
Between Nos. 2951–3049	R. & M. No. 3050 3*s.* 6*d.* (post 3*d.*)
Between Nos. 3051–3149	R. & M. No. 3150 3*s.* 6*d.* (post 3*d.*)

HER MAJESTY'S STATIONERY OFFICE

from the addresses overleaf

Printed and published by
HER MAJESTY'S STATIONERY OFFICE

To be purchased from
York House, Kingsway, London W.C.2
423 Oxford Street, London W.1
13A Castle Street, Edinburgh 2
109 St. Mary Street, Cardiff
39 King Street, Manchester 2
50 Fairfax Street, Bristol 1
35 Smallbrook, Ringway, Birmingham 5
80 Chichester Street, Belfast 1
or through any bookseller

Printed in England

S.O. Code No. 33-3401